

This article appeared in a journal published by Elsevier. The attached copy is furnished to the author for internal non-commercial research and education use, including for instruction at the authors institution and sharing with colleagues.

Other uses, including reproduction and distribution, or selling or licensing copies, or posting to personal, institutional or third party websites are prohibited.

In most cases authors are permitted to post their version of the article (e.g. in Word or Tex form) to their personal website or institutional repository. Authors requiring further information regarding Elsevier's archiving and manuscript policies are encouraged to visit:

<http://www.elsevier.com/copyright>



## Synthesis and characterization of $T[\text{Ni}(\text{CN})_4] \cdot 2\text{pyz}$ with $T = \text{Fe}, \text{Ni}$ ; $\text{pyz} = \text{pyrazine}$ : Formation of $T\text{-pyz-Ni}$ bridges

A.A. Lemus-Santana<sup>a</sup>, J. Rodríguez-Hernández<sup>a,b</sup>, M. González<sup>a</sup>, S. Demeshko<sup>c</sup>,  
M. Ávila<sup>a</sup>, M. Knobel<sup>d</sup>, E. Reguera<sup>a,\*</sup>

<sup>a</sup> Center for Applied Science and Advanced Technology, Legaria Unit, National Polytechnic Institute of Mexico, Mexico D.F., Mexico

<sup>b</sup> Institute of Materials Science and Technology, University of Havana, Cuba

<sup>c</sup> Institut für Anorganische Chemie, Georg-August-Universität Göttingen, Tammannstraße 4, 37077 Göttingen, Germany

<sup>d</sup> Institute of Physics "Gleb Wataghin", UNICAMP, 13083-970 Campinas, SP, Brazil

### ARTICLE INFO

#### Article history:

Received 10 December 2010

Received in revised form

7 June 2011

Accepted 12 June 2011

Available online 21 June 2011

#### Keywords:

Crystal chemistry

Structural study

Layered compound

Pillared solid

Spin transition

### ABSTRACT

The formation of  $T\text{-pyz-Ni}$  bridges ( $\text{pyz} = \text{pyrazine}$ ) in the  $T[\text{Ni}(\text{CN})_4] \cdot 2\text{pyz}$  series is known for  $T = \text{Mn}, \text{Zn}, \text{Cd}$  and  $\text{Co}$  but not with  $T = \text{Fe}, \text{Ni}$ . In this contribution the existence of such bridges also for  $T = \text{Fe}, \text{Ni}$  is discussed. The obtained pillared solids,  $T[\text{Ni}(\text{CN})_4] \cdot 2\text{pyz}$ , were characterized from XRD, TG, UV-Vis, IR, Raman, Mössbauer and magnetic data. Their crystal structures were refined in the orthorhombic  $Pmna$  space group from XRD powder patterns. The structural behavior of these solids on cooling down to 77 K was also studied. In the 180–200 K temperature range the occurrence of a structural transition to a monoclinic structure ( $P2_1/c$  space group) was observed. No temperature induced spin transition was observed for  $\text{Fe}[\text{Ni}(\text{CN})_4] \cdot 2\text{pyz}$ . The iron (II) was found to be in high spin electronic state and this configuration is preserved on cooling down to 2 K. The magnetic data indicate the occurrence of a low temperature weak anti-ferromagnetic interaction between  $T$  metal centers within the  $T[\text{Ni}(\text{CN})_4]$  layer. In the paramagnetic region for  $\text{Ni}[\text{Ni}(\text{CN})_4] \cdot 2\text{pyz}$ , a reversible temperature induced spin transition for the inner Ni atom was detected.

© 2011 Elsevier Inc. All rights reserved.

### 1. Introduction

The series of layered solids,  $T[M(\text{CN})_4]$ , serves as a prototype of monoatomic thickness layers containing metal centers of unsaturated coordination sphere which can be used as anchoring sites for pillars incorporation between neighboring layers. For pillar molecules ( $L$ ) of different height and formation of  $T\text{-}L\text{-}T$  bridges, 3D porous solids of tailored cavity geometry and dimension can be obtained. Such possibility has been brought up for  $T[M(\text{CN})_4]$  where  $M = \text{Ni}, \text{Pd}, \text{Pt}$ , and  $T = \text{Co}, \text{Ni}$ , with  $L = \text{pyrazine}, 4,4\text{-bipyridine}$  and  $4,4\text{'-dipyridylacetylene}$  as neutral pillars. The resulting 3D porous frameworks have been evaluated for  $\text{H}_2$  storage [1,2]. From such systems of layered compounds and using 1,2-bis(4-pyridyl)ethylene as bridge molecule also the preparation of 3D pillared solids has been reported and studied [3]. Related to the ability of the iron(2+) atom to form both high and low spin complexes, the subseries  $\text{Fe}_{1-x}\text{T}_x[M(\text{CN})_4] \cdot \text{pyz}$  with  $T = \text{Co}, \text{Ni}$  and  $M = \text{Ni}, \text{Pd}, \text{Pt}$ , has been intensively studied in order to understand the nature of their temperature stimulated

spin-crossover behavior, particularly the pronounced hysteresis loop that is observed [4–11]. The formation of bridges between different transition metals in solids using appropriate ligands represents an opportunity to obtain molecular magnets and from this fact the materials under study could also be relevant.

For  $T[\text{Ni}(\text{CN})_4] \cdot 2\text{pyz}$  with  $T = \text{Mn}, \text{Co}, \text{Zn}, \text{Cd}$  the formation of  $T\text{-pyz-Ni}$ , for the pyrazine molecule is known [12,13]. In this sub-series of pillared solids the metal centers are found with pseudo-octahedral coordination,  $T(\text{N}_{\text{CN}})_4(\text{N}_{\text{pyz}})_2$  and  $\text{Ni}(\text{C}_{\text{CN}})_4(\text{N}_{\text{pyz}})_2$ . On cooling, in the 180–200 K temperature range a reversible structural transition, from orthorhombic to monoclinic, is observed [13].

With  $T = \text{Fe}, \text{Ni}$  the formation of pillared solids from  $T[\text{Ni}(\text{CN})_4]$  layers linked by  $T\text{-pyz-Ni}$  bridges has not been previously reported. In this contribution their preparation and characterization are discussed. The formed 3D solids,  $T[\text{Ni}(\text{CN})_4] \cdot 2\text{pyz}$ , were studied from UV-vis, infrared (IR), Raman, thermogravimetric (TG), X-ray diffraction (XRD), Mössbauer, and magnetic data, and their crystal structures refined from the recorded XRD powder patterns. On cooling, in the 180–200 K temperature range these solids undergo a reversible structural transition to form low temperature monoclinic ( $P2_1/c$  space group) phases. The low temperature phases were characterized from XRD and Raman data and their crystal structures refined.

\* Corresponding author.

E-mail address: [ereguera@yahoo.com](mailto:ereguera@yahoo.com) (E. Reguera).

<sup>1</sup> On leave from Institute of Materials Science and Technology, University of Havana, Cuba.

## 2. Experimental

The samples of  $T[\text{Ni}(\text{CN})_4] \cdot 2\text{pyz}$  with  $T = \text{Fe}, \text{Ni}$ , were prepared using an already-reported synthetic route [12]. The nature of the obtained solids as-pillared compounds was established from energy-dispersed X-ray spectroscopy (EDX), IR, Raman, UV-vis, TG, Mössbauer, magnetic and XRD data.

TG curves were recorded using Q 5000 equipment (from TA Instruments) operated in dynamic rate mode where the heating rate is varied dynamically according to a ramp in response to the derivative of weight change (as derivative increases, heating rate is decreased and vice versa). The heating rates were constrained to be at the 0.001–5 K/min range with an instrumental resolution of 5. The furnace purge was nitrogen using flow rate of 100 mL/min. IR spectra were collected by the KBr pressed disk technique using an FT spectrophotometer (Spectrum One from Perkin-Elmer). UV-vis spectra were recorded with a Perkin-Elmer spectrometer using the integration sphere method.

The Raman spectra were obtained in a Dilor Labram micro-spectrometer in the 80–300 K temperature range using the 514.5 nm excitation line of an Ar laser. The laser beam was focused on the sample surface with a 50 $\times$  microscope objective. The signal was analyzed with the help of a 256 $\times$ 1024-pixel CCD detector. For the low temperature measurements the samples were mounted on the cold stage of an Oxford Microstat N. Mössbauer spectra were recorded for  $T = \text{Fe}$  between 77 K and room temperature using Wissel equipment and  $^{57}\text{Co}/\text{Rh}$  source.

XRD patterns were collected at the XPD-10B beamline at the LNLS synchrotron radiation facility (Campinas, Brazil), at room conditions and under vacuum ( $10^{-6}$  mm Hg) in the 77–300 K temperature range upon cooling and then upon heating. Details on the setting of this beamline have been reported elsewhere [14]. The experimental details are available from Supplementary information. The structural refinement from these XRD powder patterns was performed with the Rietveld method using the FullProf program [15] and pseudo-Voigt peak shape function. Peak profiles were calculated within ten times the full width at half maximum (FWHM). The background was modeled by a third-order polynomial. The interatomic C–N and Ni–C distances were constrained to take values within certain limits considering results from structural studies in the Mn, Zn, Cd analogs [12,13].

The magnetic data were collected using vibrating sample magnetometer (VMS) and MPMS-5 SQUID devices. The room temperature hysteresis loops were recorded with a sensibility of 0.1 Oe using the VMS apparatus. All the data in the 2–300 K range were collected using the MPMS-5 SQUID magnetometer operated at 50 Oe of applied field. The sample temperature was varied at a rate of 1 K  $\text{min}^{-1}$ , both on heating and on cooling. Experimental susceptibilities (the effective magnetic moments per unit formula) were corrected for diamagnetism of the constituent atoms by the use of Pascal's constants [16].

## 3. Results and discussion

### 3.1. Room temperature crystal structure

The studied compounds were found to be isostructural with the analogs of Mn, Co, Zn, Cd. Their formula unit,  $T[\text{Ni}(\text{CN})_4] \cdot 2\text{pyz}$  with  $T = \text{Fe}, \text{Ni}$  was confirmed from EDX analyses, IR, Raman spectra, and TG data. For  $T = \text{Fe}$ , from EDX spectra a Ni:Fe atomic ratio of 1:1 was obtained. IR and Raman spectra (discussed below) indicated presence of pyrazine in the obtained solids. According to the recorded TG curves (Fig. 1) a weight loss corresponding to the presence of two pyrazine molecules per formula units was observed before the layer thermal decomposition. According to

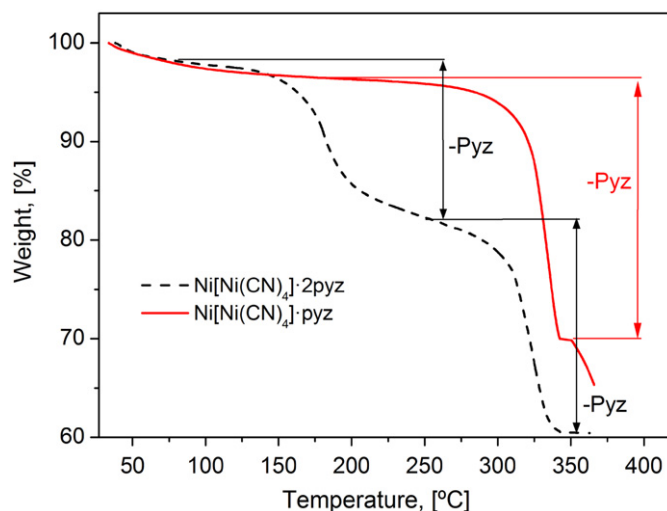


Fig. 1. TG curve for  $\text{Ni}[\text{Ni}(\text{CN})_4] \cdot 2\text{pyz}$ . An analog thermal behavior was observed for  $\text{Fe}[\text{Ni}(\text{CN})_4] \cdot 2\text{pyz}$ . For comparison, the curve for  $\text{Ni}[\text{Ni}(\text{CN})_4] \cdot \text{pyz}$  was included.

XRD, the formed solids contain a minor fraction of tetragonal phase corresponding to the mono-pyrazine pillared solid,  $T[\text{Ni}(\text{CN})_4] \cdot \text{pyz}$  [13] (see Supplementary Information). In Table 1 the unit cell parameters at room temperature for the orthorhombic phase of  $T = \text{Fe}, \text{Ni}$  are collected. Their crystal structures were refined in the  $Pmna$  space group.<sup>2</sup> The obtained structural information for these two room temperature phases is available from Supplementary Information and it was also deposited in the Cambridge Crystallographic Data Centre with the CCDC file numbers indicated below. The relevant inter-atomic distances are summarized in Table 2.

The 3D framework for the orthorhombic phases was found to be formed by rippled  $T[\text{Ni}(\text{CN})_4]$  layers which remain linked by  $T\text{-pyz-Ni}$  bridges in a crossed configuration (see Supplementary Information), similar to their Mn, Co, Zn and Cd analogs [12,13]. The two metal centers were found with pseudo-octahedral coordination,  $T(\text{N}_{\text{CN}})_4(\text{N}_{\text{pyz}})_2$  and  $\text{Ni}(\text{C}_{\text{CN}})_4(\text{N}_{\text{pyz}})_2$ , which was confirmed from the recorded UV-vis spectra (discussed below). The  $T\text{-N}_{\text{pyz}}$  distance, in Å (Table 2), follows the order  $\text{Fe} (2.310) < \text{Ni} (2.343)$ . This order finds explanation in the metal ability to accommodate charge from the ligand electron cloud in its  $d$  orbitals. The relatively weak bonding interaction established between the Ni atom in the  $[\text{Ni}(\text{CN})_4]$  unit with the pyrazine molecule is also appreciated when the bonding distances  $T\text{-N}_{\text{pyz}}$  and  $\text{Ni-N}_{\text{pyz}}$  are compared; without exception  $T\text{-N}_{\text{pyz}} < \text{Ni-N}_{\text{pyz}}$ .

The rippled sheets configuration adopted by the layers is related to the mentioned system of crossed bridges. This minimizes the inter-layers distance and, in consequence, the framework free space. The resulting pores network is formed by narrow channels of irregular shape (see Supplementary Information). For the analogs of Mn, Zn and Cd such system of narrow channels were found to be non-appropriate for storage and separation of even small molecules, e.g.  $\text{H}_2$  [12].

### 3.2. Behavior on cooling

The occurrence of a possible low temperature structural transition was explored considering the known behavior for the analogs of Mn, Co, Zn and Cd [13]. The reversible structural

<sup>2</sup> The previous assignment of the non-centrosymmetric  $Pnc2$  space group for the analogs for Mn, Co, Zn, Cd was reconsidered and the corresponding corrections introduced in the structural information deposited in ICSD and CCDC data bases.

**Table 1**  
Cell parameters for the high and low temperatures phases of  $T[\text{Ni}(\text{CN})_4] \cdot 2\text{pyz}$  with  $T = \text{Fe}, \text{Ni}$ .

Parameters	$\text{Fe}[\text{Ni}(\text{CN})_4] \cdot 2\text{pyz-RT}$	$\text{Fe}[\text{Ni}(\text{CN})_4] \cdot 2\text{pyz-77 K}$	$\text{Ni}[\text{Ni}(\text{CN})_4] \cdot 2\text{pyz-RT}$	$\text{Ni}[\text{Ni}(\text{CN})_4] \cdot 2\text{pyz-77 K}$
Cell edges, Å	$a = 7.308(2)$ $b = 6.835(3)$ $c = 14.013(2)$	$a = 6.824(2)$ $b = 13.872(3)$ $c = 7.281(2)$ $\beta = 90.4(1)^\circ$	$a = 7.247(7)$ $b = 6.769(6)$ $c = 13.836(4)$	$a = 6.728(6)$ $b = 13.732(8)$ $c = 7.231(5)$ $\beta = 90.1(3)^\circ$
Cell volume, Å <sup>3</sup>	699.9(2)	689.2(2)	678.9(3)	668.1(3)
Space group	<i>Pmna</i>	<i>P2<sub>1</sub>/c</i>	<i>Pmna</i>	<i>P2<sub>1</sub>/c</i>
Z	2	2	2	2

**Table 2**  
Relevant inter-atomic distances (in Å) for the room and low temperatures phases of  $T[\text{Ni}(\text{CN})_4] \cdot 2\text{pyz}$  with  $T = \text{Fe}, \text{Ni}$ .

Inter-atomic distance	$\text{Fe}[\text{Ni}(\text{CN})_4] \cdot 2\text{pyz-RT}$	$\text{Fe}[\text{Ni}(\text{CN})_4] \cdot 2\text{pyz-77 K}$	$\text{Ni}[\text{Ni}(\text{CN})_4] \cdot 2\text{pyz-RT}$	$\text{Ni}[\text{Ni}(\text{CN})_4] \cdot 2\text{pyz-77 K}$
$N_{\text{pyz-T}}$	2.310(2)	2.329(2)	2.343(2)	2.345(2)
$N_{\text{pyz-Ni}}$	2.857(2)	2.751(2)	2.769(2)	2.786(2)
$\langle N_{\text{CN-T}} \rangle$	2.165(2)	2.205(2)	2.189(2)	2.185(2)
$T-\text{Ni} (\text{Ni}-\text{CN}-T)$	5.003(5)	4.969(5)	4.958(5)	4.943(5)
$T-\text{Ni} (\text{Ni}-\text{pyz}-T)$	7.796(5)	7.729(5)	7.664(5)	7.646(5)
$\langle T-T (\text{layer}) \rangle$	7.071(4)	7.052(4)	7.007(5)	6.979(4)

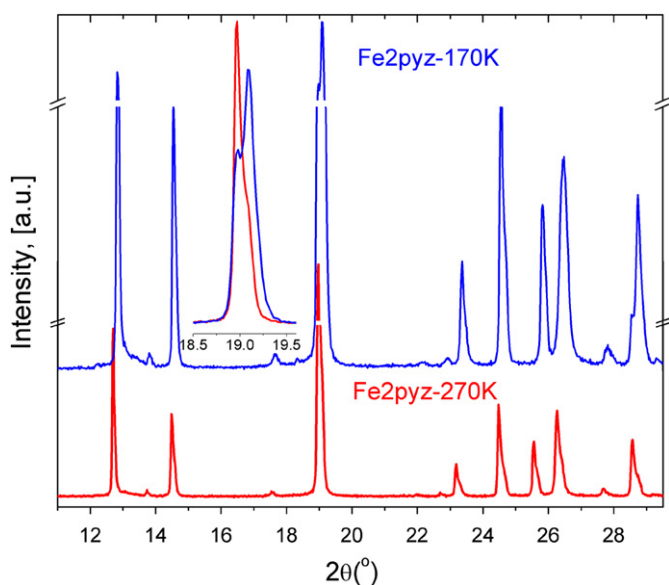


**Fig. 2.** High resolution XRD powder patterns indicating the occurrence of a low temperature structural transition in  $\text{Fe}[\text{Ni}(\text{CN})_4] \cdot 2\text{pyz}$ . The structural transition is appreciated as partial splitting of some diffraction peaks accompanied of a shift to higher angles for the diffraction pattern as a whole. An analog behavior was observed for  $\text{Ni}[\text{Ni}(\text{CN})_4] \cdot 2\text{pyz}$  (see Supplementary Information).

transition also in the 180–200 K range was detected as splitting for several diffraction peaks accompanied of a slight shift to higher diffraction angles for the pattern as a whole (Fig. 2). Such selective peak splitting corresponds to the occurrence of an anisotropic unit cell deformation. The recorded XRD powder patterns for the low temperature phases correspond to a monoclinic unit cell (*P2<sub>1</sub>/c* space group).<sup>3</sup> In Table 1 the calculated cell parameters are summarized.

The unit cell volume contraction related to the low temperature structural transition amounts (in %): 1.27 (Fe) and 1.28 (Ni). That cell volume contraction was interpreted as related to certain

<sup>3</sup> The previous assignment of the non-centrosymmetric *Pc* space group for the low temperature phase of Mn, Co, Zn, Cd analogs was reconsidered and the corresponding corrections introduced in the structural information deposited in CCDC data base.

charge redistribution within the two involved molecular blocks, the layered structure and the pyrazine molecule. The detected monoclinic deviation, relative to the orthorhombic symmetry was found to be very small (in °): Ni (90.1) and Fe (90.4). According to the observed peak splitting, the deformation is observed along the (1 1 1), (1 3 1) and (1 5 1) directions. In the low temperature monoclinic phase the (1 1 1), (−1 1 1), (1 3 1), (−1 3 1), (1 5 1) and (−1 5 1) reflections appear partially resolved (see Fig. 2).

The crystal structures for the low temperature phases were refined from high-resolution XRD powder patterns. The obtained structural information is available from Supplementary Information and it was also deposited in the Cambridge Crystallographic Data Centre with the CCDC file numbers indicated below. The relevant inter-atomic distances are summarized in Table 2.

The occurrence of a temperature induced spin transition close to room temperature is a well established phenomenon for  $\text{Fe}[\text{Ni}(\text{CN})_4] \cdot \text{pyz}$  [4–10]. For  $\text{Fe}[\text{Ni}(\text{CN})_4] \cdot 2\text{pyz}$  Mössbauer spectra were recorded in the 77–300 K range (see Supplementary Information). All the spectra are formed by two quadrupole splitting doublets (Fig. 3) related to high spin iron atoms in  $\text{Fe}[\text{Ni}(\text{CN})_4] \cdot 2\text{pyz}$  (main phase) and low spin Fe(II) in  $\text{Fe}[\text{Ni}(\text{CN})_4] \cdot \text{pyz}$  (minor phase, ~8%). The high spin state for the iron atom was preserved on cooling down to 77 K. In Table 3 the values for the fitted Mössbauer parameters, isomer shift ( $\delta$ ), quadrupole splitting ( $\Delta$ ) and linewidth ( $\Gamma$ ) are summarized. The observed variation in the value of  $\delta$  was ascribed to the second order temperature Doppler effect with probably a small contribution related to the structural transition detected by XRD in the 180–200 K temperature range. The detected systematic increase for the value of  $\Delta$  on cooling confirms the high spin electronic configuration for the iron atom. Low spin iron (II) is practically insensitive to a temperature change. An analog result is obtained from magnetic measurements in the 2–300 K temperature range (discussed below).

### 3.3. Thermal stability on heating

Fig. 1 shows the recorded TG curve for the sample of  $\text{Ni}[\text{Ni}(\text{CN})_4] \cdot 2\text{pyz}$ , which is representative for the two compositions under study. For comparison the thermogram for  $\text{Ni}[\text{Ni}(\text{CN})_4] \cdot \text{pyz}$  was included. The small weight lost observed below 80 °C for  $\text{Ni}[\text{Ni}(\text{CN})_4] \cdot 2\text{pyz}$  was ascribed to the presence of

a small fraction of tetragonal phase. The tetragonal structure has cavities of about  $4.5 \times 8.5 \text{ \AA}$ , enough to accommodate weakly bonded water molecules. The tetragonal phase has been reported as dihydrate [3–10] while the orthorhombic one is obtained as an anhydrous solid [12,13]. The orthorhombic phase loses the two pyrazine molecules in two steps, from about 130 and 205 °C (Fig. 1), with formation of an intermediate mono-pyrazine solid, a behavior already observed for the analogs of Mn, Zn and Cd [12]. The tetragonal phase shows a higher thermal stability; its pyrazine molecule evolves from about 240 °C (Fig. 1). Such difference of thermal stability for the orthorhombic and tetragonal phases was interpreted as related to the participation of  $[\text{Ni}(\text{CN})_4]$  molecular orbitals above and below the square plane,

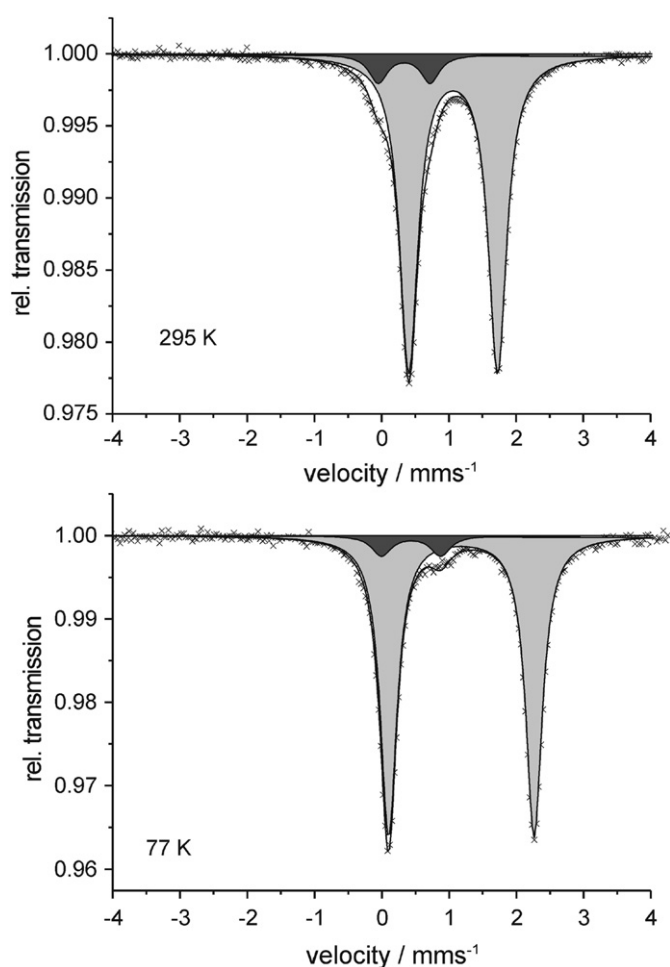


**Fig. 3.** Mössbauer spectra at 295 and 77 K for  $\text{Fe}[\text{Ni}(\text{CN})_4] \cdot 2\text{pyz}$ . The most intense doublet corresponds to high spin Fe (II) in  $\text{Fe}[\text{Ni}(\text{CN})_4] \cdot 2\text{pyz}$  (light gray area). No temperature induced spin transition was observed for this compound. The sample also contains about 8% of  $\text{Fe}[\text{Ni}(\text{CN})_4] \cdot \text{pyz}$  (low spin Fe(II), dark gray area).

**Table 3**

Mössbauer parameters at different temperatures for  $\text{Fe}[\text{Ni}(\text{CN})_4] \cdot 2\text{pyz}$ .

Temperature, (K)	$\delta^a$ , (mm/s)		$\Delta$ , (mm/s)		$\Gamma$ , (mm/s)		A, (%)	
	HS-Fe <sup>II</sup>	LS-Fe <sup>II</sup>						
295	1.06	0.34	1.32	0.77	0.33	0.33	91.7	8.3
250	1.10	0.36	1.47	0.78	0.33	0.35	91.7	8.3
150	1.15	0.41	1.93	0.85	0.31	0.35	91.6	8.4
77	1.18	0.43	2.16	0.88	0.30	0.35	92.7	7.3

<sup>a</sup> The value of  $\delta$  is reported relative to  $\alpha$ -Fe. Fitting error in  $\delta$ ,  $\Delta$ , and  $\Gamma$  is no higher than 0.01 mm/s.

which yields to the weakening of the resulting structure. The strength of pyrazine molecule binding to the Ni atom is relatively weak. This is supported by the refined crystal structures where the following order for the bonding distance is observed,  $T\text{-N}_{\text{pyz}} < \text{Ni}\text{-N}_{\text{pyz}}$  (already discussed).

### 3.4. UV-vis, IR and Raman characterization

UV-vis spectra recorded at room temperature (Fig. 4) were used as sensor for the metal coordination mode. With  $T = \text{Mn, Zn}$ , two metals without  $d-d$  transitions, the distorted octahedral geometry for Ni has been previously identified by the presence of broad and weak absorption bands in the 500–1000 nm region [12]. Accordingly, with  $T = \text{Fe, Ni}$ , the appearance of absorption bands from the two metal centers ( $T, \text{Ni}$ ) in octahedral coordination was expected. Because of the slightly different coordination environments for the metal centers ( $T(\text{N}_{\text{CN}})_4(\text{N}_{\text{pyz}})_2$  and  $\text{Ni}(\text{C}_{\text{CN}})_4(\text{N}_{\text{pyz}})_2$ ), these transitions appear overlapped and lead to the broad absorption observed in the visible region (Fig. 4). In the bi-pyrazine composition, electronic transitions from octahedral Fe(II) in  $\text{Fe}[\text{Ni}(\text{CN})_4] \cdot 2\text{pyz}$  prevails on Ni(II) electronic transitions, since there is no coincidence among observed bands. The spectrum of  $\text{Fe}[\text{Ni}(\text{CN})_4] \cdot 2\text{pyz}$  shows a broad band in the visible region centered at 774 nm, in agreement with the expected  ${}^5E_g \leftarrow {}^5T_{2g}$  transition in high-spin octahedral complexes of Fe(II) [17]. The broadening of this single band is explained by a distorted octahedral symmetry or a Jahn-Teller effect in its excited state. This latter

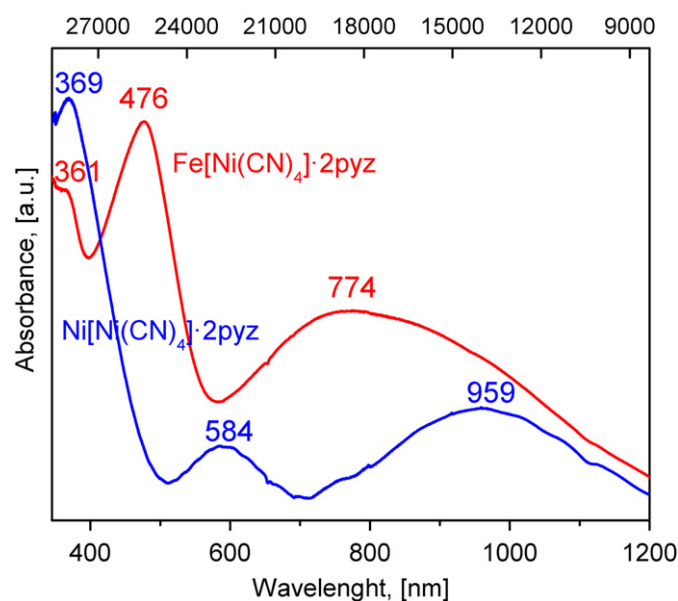


**Fig. 4.** UV-vis spectra for  $\text{Fe}[\text{Ni}(\text{CN})_4] \cdot 2\text{pyz}$  and  $\text{Ni}[\text{Ni}(\text{CN})_4] \cdot 2\text{pyz}$ . The observed bands correspond to transitions for the involved metals ( $T, \text{Ni}$ ) in pseudo-octahedral coordination.

effect could be responsible for the splitting of the mentioned transition, allowing the more energetic band at 476 nm. This band is close to UV region and its intensity suggests that it results from a charge-transfer transition [17]. Because of the asymmetrical *T*-pyz-Ni bridge the inner metal (Ni) is found with a distorted pseudo-octahedral geometry, which can be identified in the UV-vis spectrum of  $\text{Ni}[\text{Ni}(\text{CN})_4] \cdot 2\text{pyz}$ . Ni(II) centers in this compound, are both octahedral, thus the spectrum shows two transitions at 959 and 584 nm (Fig. 4), which were ascribed to two of the three spin-allowed transitions for octahedral Ni atom [17].

IR and Raman spectra are excellent sensor for the pyrazine molecule coordination to the metal centers [18]. The coordination bond formation with the pyrazine molecule involves the charge donation to the metal centers, with the corresponding charge redistribution within the pyrazine molecule ring and in the  $T[\text{Ni}(\text{CN})_4]$  layer. Such charge redistribution is sensed by changes in the vibrational spectra of these building blocks. Free pyrazine exhibits weak  $\nu(\text{C-H})$  bands at 3083–2972  $\text{cm}^{-1}$  but these vibrations shift to the 3110–3035 and 3120–2930  $\text{cm}^{-1}$  regions when the orthorhombic structure is formed (Fig. 5 and Table 4). The

$\gamma(\text{CH})$  and  $\delta(\text{CH})$  vibrations within the pyrazine ring also sense the charge subtraction on the pyrazine coordination to the metal (see Supporting information). The asymmetrical *T*-pyz-Ni bridges formation is also detected as two non-equivalent vibrations for the  $\gamma_{\text{ring}}$  mode, accompanied of a frequency increase in the 30 and 65  $\text{cm}^{-1}$  range relative to free pyrazine (Fig. 5 and Table 4). Within the layer the coordination bond formation with pyrazine is sensed as frequency shifts for the  $\nu(\text{CN})$ ,  $\nu(\text{Ni-C})$  and  $\delta(\text{Ni-C-N})$  vibrations, the most pronounced ones being those observed for the  $\nu(\text{CN})$  mode. Probably the simplest sensor for the pillar molecule incorporation between neighboring layers is the frequency shift for the  $\nu(\text{CN})$  vibration. Regarding the  $T[\text{Ni}(\text{CN})_4] \cdot x\text{H}_2\text{O}$  layers, the *T*-pyz-Ni bridge formation leads to a shift toward the low frequency region for the  $\nu(\text{CN})$  vibration, which amounts  $-8$  (Fe) and  $-18$  (Ni)  $\text{cm}^{-1}$  (Table 4). The shift is toward the opposite side (higher frequency region) for the tetragonal phases,  $+19$  (Fe) and  $+7$  (Ni)  $\text{cm}^{-1}$  (Table 4). Such difference of behavior sheds light on the nature of the pyrazine molecule interaction with the metal centers. The *T*-pyz-Ni coordination involves certain charge donation from pyrazine

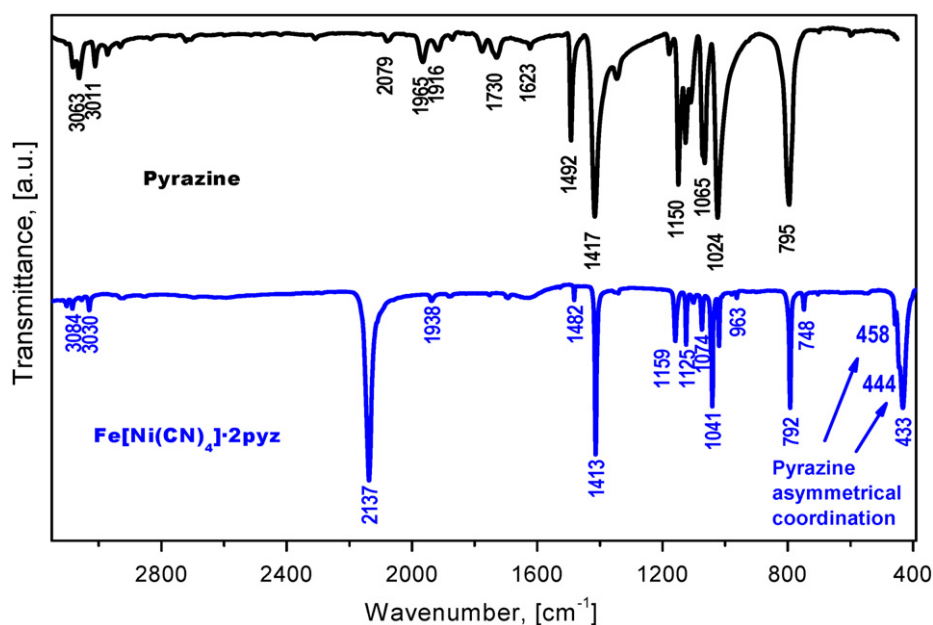


Fig. 5. IR spectrum (2600–400  $\text{cm}^{-1}$  region) for  $\text{Fe}[\text{Ni}(\text{CN})_4] \cdot 2\text{pyz}$ . For comparison, the spectrum of free pyrazine is included. An analog spectrum is obtained for  $\text{Ni}[\text{Ni}(\text{CN})_4] \cdot 2\text{pyz}$  (see Supplementary Information).

**Table 4**  
Frequency (in  $\text{cm}^{-1}$ ) for the IR and Raman spectral signals relevant as sensor for the pyrazine (pyz) molecule coordination in the high (HT) and low (LT) temperature phases of  $T[\text{Ni}(\text{CN})_4] \cdot 2\text{pyz}$ . For comparison, the IR and Raman data for the tetragonal phases are included.

Vibration	<i>T</i> · xpyz								
	Fe · 2pyz RT	Fe · 2pyz LT	Fe · pyz RT	Fe · pyz LT	Ni · 2pyz RT	Ni · 2pyz LT	Ni · pyz RT	Ni · pyz LT	$[\text{Ni}(\text{CN})_4]$ RT
$\nu(\text{CN})^a$	2137s	–	2173s	–	2147	–	2172	–	2122s
$\nu(\text{CN})^b$	2183sh	2190sh	2197s	2201s	2191sh	2191sh	2192s	2194s	2133s
	2162s	2164s	2185sh	2189sh	2166s	2169s	2182sh	2183sh	
$\delta(\text{Ni-C-N})^a$	433m	–	444m	–	436m	–	445m	–	418m
$\delta(\text{Ni-C-N})^b$	466w	464w	483w	495w	465w	465w	483w	noise	395w
$\nu(\text{T-N}_{\text{CN}})^b$	345w	347w	344w	344w	341w	344w	333w	340w	–
$\nu(\text{T-N}_{\text{pyz}})^b$	noise	225w	269w	271w	255w	255w	263w	265w	–
		$\text{Fe}[\text{Ni}(\text{CN})_4] \cdot x\text{H}_2\text{O}$ RT				$\text{Ni}[\text{Ni}(\text{CN})_4] \cdot x\text{H}_2\text{O}$ RT			
		2154				2166			

RT=room temperature; LT=low temperature.

<sup>a</sup> IR frequency.

<sup>b</sup> Raman frequency; s=strong; sh=shoulder; m=medium; w=weak.

molecule to  $a_{2u}$  orbital, the most important  $\pi$ -molecular orbital for the  $[\text{Ni}(\text{CN})_4]$  unit. Such interaction contributes to a decrease for the  $\nu(\text{CN})$  stretching frequency. The  $a_{2u}$  orbital is a mixture of  $4p_z$  metal orbital and the four ligand  $\pi_\nu$ -orbitals ( $\nu$  means vertical to the square plane) which has anti-bonding character. The mixing of the  $a_{2u}$  orbital and the low-lying energy pyrazine  $\pi^*$  orbitals with their concomitant population upon the  $T$ -pyz-Ni bridge formation, explains the red shift detected for the  $\nu(\text{CN})$  vibration and also the above discussed lower thermal stability observed for the orthorhombic phases [18].

The above-discussed structural transition on cooling for the orthorhombic phases was explored from Raman spectra. The variation observed in frequency for the  $\nu(\text{CN})$  vibration is relatively small, of only about  $+3 \text{ cm}^{-1}$  (Table 4). This corresponds to a slight enhancement for the  $\text{C}\equiv\text{N}$  bond, probably related to an increase of electron density on the metal  $T$  which induces a reduction for the  $\pi$ -back bonding interaction from the Ni atom toward the CN ligand. The slight variation in frequency for that vibration agrees with the above discussed small unit cell volume contraction associated to the structural transition. This structural transition does not involve dramatic change in the framework electron density.

### 3.5. Magnetic measurements

Fig. 6 shows the thermal dependence of the  $\chi_M T$  product (where  $\chi_M$  is the molar magnetic susceptibility and  $T$  the temperature) for both  $T=\text{Fe}, \text{Ni}$ . The remaining magnetic data and their temperature dependence are available from the Supplementary Information file. Above 50 K the observed magnetic behavior corresponds to materials in paramagnetic state. Below that temperature a progressive anti-ferromagnetic interaction is detected with Curie–Weiss ( $\theta_{\text{CW}}$ ) constant values of  $-3.04$  and  $-1.04$  K for Fe and Ni, respectively (see Supplementary Information). Such small absolute  $\theta_{\text{CW}}$  values suggest a low spin (diamagnetic) electronic configuration for the Ni atom in the  $[\text{Ni}(\text{CN})_4]$  unit resulting into an anti-ferromagnetic interaction between  $T$  metals distant about  $10 \text{ \AA}$ . Similar small  $\theta_{\text{CW}}$  values have been observed for  $\text{Fe}(\text{III})\text{-C}\equiv\text{N-Zn-N}\equiv\text{C-Fe}(\text{III})$  chains in zinc hexacyanoferrate (III) [19].

For  $\text{Fe}[\text{Ni}(\text{CN})_4] \cdot 2\text{pyz}$  no significant variation is observed for  $\chi_M T$  product on cooling from 300 down to 50 K, it shows a slight decrease, from  $3.35$  to  $3.22 \text{ cm}^3 \text{ mol}^{-1} \text{ K}$ . When the obtained values for  $\chi_M$  are converted to effective magnetic moment ( $\mu_{\text{eff}}$ ) per formula unit, considering the diamagnetism correction [16],

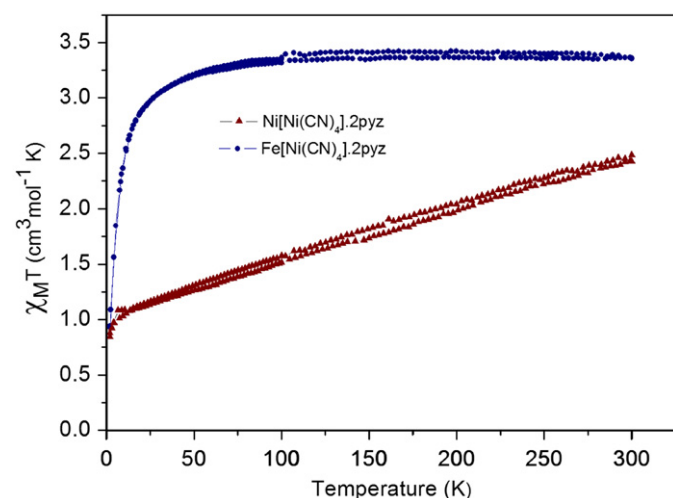


Fig. 6. Magnetic behavior in the form of  $\chi_M T$  vs.  $T$  curves for  $\text{Ni}[\text{Ni}(\text{CN})_4] \cdot 2\text{pyz}$  and  $\text{Fe}[\text{Ni}(\text{CN})_4] \cdot 2\text{pyz}$  powders upon heating and cooling.

$\mu_{\text{eff}}=5.11 \text{ MB}$  is obtained for the two temperatures (300 and 50 K). This  $\mu_{\text{eff}}$  value corresponds to four unpaired electrons per formula unit, which suggests that for  $T=\text{Fe}$  the Ni atom in the  $[\text{Ni}(\text{CN})_4]$  unit is found in a low spin (diamagnetic) state for all the temperature range, 2–300 K. The iron (II) atom is found in high spin state for all the explored temperature range, 2–300 K. This is also explained by the flat feature observed for the  $\chi_M T$  vs.  $T$  curve in the paramagnetic region for  $\text{Fe}[\text{Ni}(\text{CN})_4] \cdot 2\text{pyz}$ , a result that is in accordance with the above discussed Mössbauer spectra.

For  $\text{Ni}[\text{Ni}(\text{CN})_4] \cdot 2\text{pyz}$  the  $\chi_M T$  vs.  $T$  dependence shows a monotonous decreasing behavior. The effective magnetic moment ( $\mu_{\text{eff}}$ ) per formula unit changes from  $4.27 \text{ MB}$  at 300 K to  $3.04 \text{ MB}$  at 50 K. These values correspond to 3 and 2 unpaired electrons per formula unit, respectively. Below 50 K the Ni atom in the  $[\text{Ni}(\text{CN})_4]$  unit is found in a low spin (diamagnetic) state ( $S=0$ ) and only the outer metal (Ni) is contributing to the value of  $\mu_{\text{eff}}$ . Above 50 K a temperature induced dynamic spin transition, between high and low spin states,  $S=1$  and  $S=0$ , is responsible for the observed  $\chi_M T$  vs.  $T$  dependence. It seems, the energy barrier height between these two states in the pseudo-octahedral environment for Ni(II),  $\text{Ni}(\text{C}_{\text{CN}})_4(\text{N}_{\text{pyz}})_2$ , is similar to the thermal energy,  $kT$ . This hypothesis is supported by the refined crystal structures. The Ni– $\text{N}_{\text{pyz}}$  distance for  $\text{Ni}[\text{Ni}(\text{CN})_4] \cdot 2\text{pyz}$  varies from  $2.769(2) \text{ \AA}$  at 300 K to  $2.786(2) \text{ \AA}$  at 77 K (see Table 2). On cooling a progressive weakening for the Ni-pyrazine bond takes place and this favors a diamagnetic electronic configuration for the inner Ni atom. This is a reversible temperature induced process because no hysteresis on heating was observed (see Supplementary). The behavior for  $\text{Fe}[\text{Ni}(\text{CN})_4] \cdot 2\text{pyz}$  is quite different, at low temperature the Ni-pyrazine bond becomes stronger (see Table 2).

## 4. Conclusions

For  $T[\text{Ni}(\text{CN})_4] \cdot 2\text{pyz}$  with  $T=\text{Fe}, \text{Ni}$ , the formation of  $T$ -pyz-Ni bridges was identified from XRD, TG, IR and UV–vis data. These solids crystallize with an orthorhombic unit cell ( $Pmna$ ) with a framework formed of rippled  $T[\text{Ni}(\text{CN})_4]$  layers linked by crossed  $T$ -pyz-Ni bridges; a structural feature already observed for the analogs of Mn, Co, Zn and Cd. Compared to the series where  $T$ -pyz- $T$  bridges are formed (tetragonal,  $P4/m$ ), the orthorhombic structure shows a lower thermal stability. Such behavior was ascribed to the formation of a relatively weak  $\text{N}_{\text{pyz}}\text{-Ni}_{\text{CN}}$  bond. On cooling, in the temperature region of 180–200 K, a reversible structural transition is observed. From the orthorhombic phase a low temperature monoclinic phase ( $P2_1/c$  space group) is formed. Such structural transition is appreciated as a slight monoclinic distortion for the orthorhombic structure, involving a unit cell volume reduction of about 1.3%. The crystal structures for both, the room and low temperature, phases were refined from the recorded XRD powder patterns. The recorded Raman spectra suggest that the structural transition has associated only slight changes in the electronic structure of the solids. No occurrence of temperature induced spin transition was observed for  $\text{Fe}[\text{Ni}(\text{CN})_4] \cdot 2\text{pyz}$ . The iron (II) is found to be in high spin electronic state and this configuration is preserved on cooling down to 2 K. For the nickel atom in the pseudo-octahedral environment,  $\text{Ni}(\text{C}_{\text{CN}})_4(\text{N}_{\text{pyz}})_2$ , a dynamic temperature induced spin transition was detected within the paramagnetic region. At low temperature,  $< 50 \text{ K}$ , in both  $\text{Fe}[\text{Ni}(\text{CN})_4] \cdot 2\text{pyz}$  and  $\text{Ni}[\text{Ni}(\text{CN})_4] \cdot 2\text{pyz}$ , a weak anti-ferromagnetic interaction between  $T$  metal centers within the  $T[\text{Ni}(\text{CN})_4]$  layer was observed.

## Supplementary information

This file contains XRD, IR, Raman, Mössbauer and magnetic data for the studied compounds. Structural information derived from the

crystal structures refinement has also been deposited at the Cambridge Crystallographic Data Centre (e-mail: deposit@ccdc.cam.ac.uk) with CCDC file numbers: 753599: Fe[Ni(CN)<sub>4</sub>] · 2pyz (RT); 753600: Fe[Ni(CN)<sub>4</sub>] · 2pyz (77 K); 753603: Ni[Ni(CN)<sub>4</sub>] · 2pyz (RT); 753604: Ni[Ni(CN)<sub>4</sub>] · 2pyz (77 K).

### Acknowledgment

This work was partially supported by the Project SEP-CON-ACyT-2009-01-129048. The access to the LNLS Brazilian synchrotron light radiation facility is greatly recognized. The authors thank Prof. Dr. F. Meyer (from Institut für Anorganische Chemie, Georg-August-Universität Göttingen, Germany) for the access to the Mössbauer spectroscopy facility.

### Appendix A. Supplementary material

Supplementary data associated with this article can be found in the online version at doi:10.1016/j.jssc.2011.06.011.

### References

- [1] Y. Li, Y. Liu, Y. Wang, Y. Leng, L. Xie, X. Li, *Int. J. Hydrog. Energy* 32 (2007) 3411.
- [2] J.T. Culp, S. Natesakhawat, M.R. Smith, E. Bittner, C. Matranga, B. Bockrath, *J. Phys. Chem. C* 112 (2008) 7079.
- [3] J.T. Culp, M.R. Smith, E. Bittner, B. Bockrath, *J. Am. Chem. Soc.* 130 (2008) 12427.
- [4] V. Niel, J.M. Martínez-Agudo, M.C. Muñoz, A.B. Gaspar, J.-A. Real, *Inorg. Chem.* 40 (2001) 3838.
- [5] G. Molnár, V. Niel, A.B. Gaspar, J.-A. Real, A. Zwick, A. Bousseksou, J.J. McGarvey, *J. Phys. Chem. B* 106 (2002) 9701.
- [6] G. Molnár, V. Niel, J.-A. Real, L. Dubrovinsky, A. Bousseksou, J.J. McGarvey, *J. Phys. Chem. B* 107 (2003) 3149.
- [7] G. Molnár, T. Kitazawa, L. Dubrovinsky, J.J. McGarvey, A. Bousseksou, *J. Phys.: Condens. Matter* 16 (2004) S1129.
- [8] T. Tayagaki, A. Galet, G. Molnár, M.C. Muñoz, K. Tanaka, J.-A. Real, A. Bousseksou, *J. Phys. Chem. B* 109 (2005) 14859.
- [9] S. Cobo, D. Ostrovskii, S. Bonhommeau, L. Vandier, G. Molnár, L. Salmon, K. Tanaka, A. Bousseksou, *J. Am. Chem. Soc.* 130 (2008) 9019.
- [10] G. Agustí, S. Cobo, A.B. Gaspar, G. Molnár, N.O. Moussa, P.A. Szilágyi, V. Pálfi, C. Vieu, M.C. Muñoz, J.-A. Real, A. Bousseksou, *Chem. Mater.* 20 (2008) 6721.
- [11] P.D. Southom, L. Liu, E.A. Fellows, D.J. Price, G.J. Halder, K.W. Chapman, B. Moubaraki, K.S. Murray, J.-F. Létard, C.J. Kepert, *J. Am. Chem. Soc.* 131 (2009) 10998.
- [12] A.A. Lemus-Santana, J. Rodríguez-Hernández, L.F. Del Castillo, M. Basterrechea, E. Reguera, *J. Solid State Chem.* 182 (2009) 757.
- [13] J. Rodríguez-Hernández, A.A. Lemus-Santana, J. Ortiz-López, S. Jiménez-Sandoval, E. Reguera, *J. Solid State Chem.* 183 (2010) 105.
- [14] F.F. Ferreira, E. Granado, W. Carvalho Jr., S.W. Kycia, D. Bruno, R. Droppa Jr., *J. Synchrotron Radiat.* 13 (2006) 46.
- [15] J. Rodríguez-Carvajal, FullProf 2005 Program, Institute Louis Brillouin, Saclay, France, 2005.
- [16] R.S. Drago, *Physical Methods for Chemists*, 2nd ed., Saunders College Publishing, Gainesville, 1962 Chapter 11.
- [17] N.N. Greenwood, A. Earnshaw, *Chemistry of the elements*, 2nd ed., Butterworth-Heinemann, Great Britain, 1998.
- [18] K. Nakamoto, *Infrared and Raman Spectra of Inorganic and Coordination Compounds*, John-Wiley & Sons, New York, Chichester, Brisbane, Toronto, Singapore, 1995.
- [19] R. Martínez-García, M. Knobel, E. Reguera, *J. Phys. Chem. B* 110 (2006) 7296.